Author Version of : Science of The Total Environment, vol.892; 2023; Article no: 164680

Link of the short-term temporal trends of Sr and Nd isotopic composition of aeolian dust over the Arabian Sea with the source emissions

Srinivas Bikkina [a], Arvind Shukla [a,b], Sunil Kumar Singh [a,c]*, Damodaraorao Karri [d], Naman D. Singh [a], and Bisweswar Sahoo [e]

[a] CSIR-National Institute of Oceanography, Dona-Paula, Goa, India-403004,
[b] School of Earth Ocean and Atmospheric Sciences, Goa University, Goa, India-403004
[c]Academy of Scientific and Innovative Research (AcSIR), Kamla Nehru Nagar, Ghaziabad, Uttar Pradesh 201002, India
[d] Department of Earth Sciences, IISER Kolkata, India-741246
[e] School of Earth, Ocean, and Climate Sciences, IIT Bhubaneswar, India-752050
*Corresponding author: sunil@nio.org; sunilsingh160371@gmail.com;

Abstract

The long-range atmospheric transport of mineral dust from the Middle East and South Asia to the Arabian Sea (AS) is an important route for delivering key trace metals and nutrients. Despite being surrounded by many deserts/land masses, it is not clear which dust source is most likely contributing to mineral aerosols over the AS in the winter season. Substantial information related to dust source emissions and transport pathways over the AS is, thus, needed for better constraining the biogeochemical effects in the sunlit surface waters. Here, we investigated the radiogenic Sr and Nd isotopic composition ($^{87}Sr/^{86}Sr$ and $\varepsilon_{Nd}(0)$), respectively) of dust samples collected over the AS during a recent GEOTRACES winter expedition (GI-10: 13 January-10 February 2020). The $^{87}Sr/^{86}Sr$ ratios of dust samples from the AS varied between 0.70957 and 0.72495, whereas the $\varepsilon_{Nd}(0)$ ranged between -24.0 and -9.3. These proxies were further tagged with their source profiles of surrounding land masses in the Middle East and India based on the origin of air mass back trajectories. We also encountered two dust storm (DS) events, one on 27 January 2020 (DS1) and the second one on 10 February 2020 (DS2), which showed the distinct isotopic composition of both tracers over the Arabian Sea. The DS1 is characterized by somewhat enriched ^{143}Nd ($\varepsilon_{Nd}(0)$: -9.3) and depleted ^{87}Sr ($^{87}Sr/^{86}Sr$: 0.70957), whereas as DS2 had relatively low $\varepsilon_{Nd}(0)$(-12.5) and high $^{87}Sr/^{86}Sr$ (0.7143). The DS1 indicated its origin in the Arabian Peninsula, and DS2 mostly evolved from Iran and the Indo-Gangetic Plain (IGP) in northern India/Pakistan. Furthermore, the Sr and Nd isotope composition of DS1 resembles with the four dust samples collected over the pelagic waters in the Arabian Sea, thus, signifies the importance of dust outbreaks from the Arabian Peninsula contributing mineral aerosol to the central Arabian Sea in the winter season. Such documentation based on the Sr and Nd isotope composition from this marine region is, hitherto, lacking in the literature and, thus, highlights the need for more measurements.

Keywords: Mineral dust, Aerosols, Sr-Nd Isotope, NE Monsoon, Arabian Sea

Graphic abstract

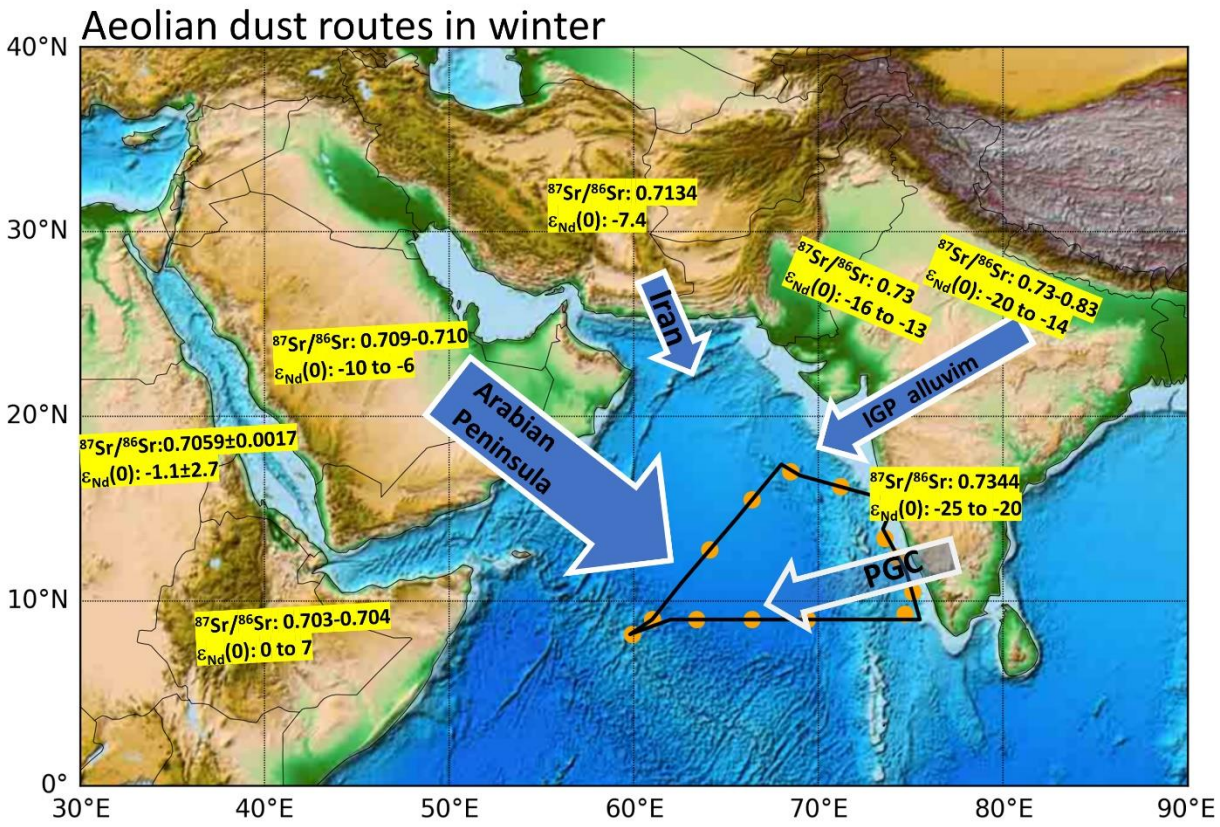

Introduction

Mineral dust is a well-known carrier of nutrients and trace metals to the marine atmosphere, and subsequent deposition to the ocean surface significantly influences the biogeochemical cycles of C and N through photosynthesis and N-fixation (Duce et al., 1991; Schulz et al., 2012; Mahowald et al., 2017). As such, the dust cycle is rather complex due to the highly sporadic and episodic nature of emissions from the deserts and their geographical extent and the atmospheric circulation pattern over the dust source regions (Choobari et al., 2014; Jickells et al., 2014). Besides, the inherent variability in the mineralogical composition associated with different continental sources further compounds the modelling efforts of dust emissions. As a result, existing studies focusing on the dust impact on oceanic biogeochemistry have, to date, relied mostly upon the chemical transport models (Keith Moore et al., 2006).

Although debatable, there is some evidence that the dust deposition to surface waters that are downwind of desert regions triggers the phytoplankton blooms (Shi et al., 2012; Banerjee and Prasanna Kumar, 2014). For instance, Wang et al. (2012) have examined the role of Asian dust transported to East China during the spring season in enhancing primary productivity based on the long-term, a multiyear record of satellite observations of chlorophyll-a and aerosol (PM_{10}) concentrations. Likewise, the sediment trap records from the 3000 m water depth over the high dust-prone regions of the North Atlantic gyre revealed significant enrichment in the particulate organic carbon fluxes compared to the South Atlantic gyre, which is less affected by the dust deposition (Pabortsava et al., 2017). Likewise, Basu et al. (2019) have shown that symbiotic bacteria associated with Trichodesmium colonies maintain the pool of dissolved iron from the mineral dust in the surface waters through the release of metal-binding organic compounds and subsequent photochemical reactions in the aqueous media. Recently, Guieu et al. (2019) observed a significant increase in the standing stocks of phytoplankton biomass in the surface waters of the Arabian Sea as a result of the response of the biogeochemical model simulations coupled with atmospheric dust dissolution schemes. Ito et al. (2016) have modelled the net effect of atmospheric processing of Asian dust in the continental outflow to the western North Pacific, and subsequent deposition to the ocean surface could stimulate phytoplankton primary productivity, which in turn has a consequence for expanding the oxygen minimum zone (OMZ). All these studies have underscored the importance of aeolian dust in the surface ocean biogeochemistry and, thereby, emphasized a need for better constraining their sources and transport pathways. The present study is a step forward in this direction and deals mainly with the provenance of atmospheric dust over the Arabian Sea. The Arabian Sea receives a substantial amount of mineral dust from the deserts of the Arabian Peninsula, Iraq, Iran, Pakistan, and India through the

shamal winds, mostly in the summer season (Pease et al., 1998; Tindale and Pease, 1999; Banerjee and Kumar, 2016; Ramaswamy et al., 2017). For instance, Jickells et al. (2005) have estimated that the deserts surrounding the Arabian Sea could contribute to ~50 g m^{-2} yr^{-1} of mineral dust load to the surface waters. The mineral aerosol particles generated from these surrounding continental sources of the Arabian Sea are rather diverse in terms of mineralogy as well as radiogenic Sr and Nd isotopic composition (Sirocko, 1994; Kumar et al., 2020; Suresh et al., 2021). A conservative information about source regions of aeolian dust can be obtained by determining the isotopic ratios of $^{87}Sr/^{86}Sr$ and $^{144}Nd/^{143}Nd$ in the detrital silicate fraction of the aeolian dust (Goldstein et al., 1984). Therefore, our goal here is to understand the probable source regions of mineral aerosols over the Arabian Sea using the Sr and Nd isotope composition of dust samples collected during a winter cruise (SSD069: 13 January – 10 February 2020).

Materials and methods

Site description

Arabian Sea (AS), the western limb of the northeastern Indian Ocean, is a biologically productive marine basin (Madhupratap et al., 1996; Patra et al., 2007). Being surrounded by several deserts, including the Gulf of Oman, Somalia, Arabian Peninsula, Iran, and the Thar regions, AS receives ample dust perennially from these source regions (Duce et al., 1991; Jickells et al., 2005). In addition, this marine basin is also influenced by the air pollutants and fine alluvium from the Indo-Gangetic Plain in winter and spring seasons (Kumar et al., 2008; Bikkina and Sarin, 2012; Bikkina et al., 2012; Aswini et al., 2020b). As a consequence, several researches have employed the chemical composition of marine aerosols (Siefert et al., 1999; Tindale and Pease, 1999; Bikkina et al., 2020), in situ hydrographic parameters (*e.g.*, Chlorophyll-a, nutrients, primary productivity, salinity, and temperature) (Patra et al., 2007), as well as satellite observations (Prospero et al., 2002; Badarinath et al., 2010) to understand the overall impact of mineral dust on the surface waters of the AS (Banerjee and Prasanna Kumar, 2014; Guieu et al., 2019; Suresh et al., 2021). But no such reports exist to date for the source apportionment of mineral dust based on the Sr and Nd isotopic composition of marine aerosols collected over the AS during the winter monsoon.

Methods

This study includes Sr and Nd isotopic composition data of dust samples collected onboard R/V Sindhu Sadhana during the two GEOTRACES-India follow-up research expeditions in the Arabian Sea during the Northeast monsoon. The cruise started from Mormugao, Goa in India, on 13 January 2020 and reached back to this port on 10 February 2020 (Figure 1). Overall, we collected a total of thirteen bulk

total suspended particulate (TSP) samples on 8" × 10" Tissuquartz filters (PALL Life Sciences Inc.) using the high-volume air sampler (Envirotech®TM; *flowrate*: 1.13 m^3 min^{-1}). The air sampler was installed onboard the front deck of the bridge of the R/V Sindhu Sadhana (SSD069/GI-10) and was operated only when the ship was cruising at a speed of over 8-10 knots per hour. Immediately after collection, all the dust samples were wrapped in prebaked Aluminum foils, sealed in airtight Ziploc bags, and stored at -19 °C until analysis.

Briefly, ~200 cm^2 filter cut of the aerosol sample was first washed with ultra-pure deionized water (Milli-Q®TM, Specific resistivity = 18.2 MΩ-cm) to remove sea salt and subsequently treated with 0.6 M HCl to remove the carbonate content of dust. Thereafter, the residual filter was washed with ultrapure water to remove the acidity, and the residue was digested with supra pure HF, HNO_3, and HCl at 110 °C for 24 h in a trace metal-free clean lab facility, under the Class 100 working environment, at the National Institute of Oceanography (NIO), Goa. This step has been repeated two to three times to ensure complete digestion. The solution was evaporated and redissolved in 4 ml of HCl. Of these, 2 ml of digested aliquot was processed to extract pure Sr and REEs using AG50W-X8 resin (200-400 mesh). Pure Nd was extracted from REEs using a lanthanum specific resin (Eichrome ® LN resin (50–100 μm) following the protocols described in Singh et al. (2008). These purified fractions of Sr and Nd were measured for their isotope composition using the multi-collector inductively coupled plasma spectrometer (MC-ICPMS; NU Plasma III) in static mode at CSIR-NIO, Goa. Mass-dependent fractionations for Sr and Nd were corrected by normalizing $^{86}Sr/^{88}Sr$ to 0.1194 and $^{146}Nd/^{144}Nd$ to 0.7219, respectively. In addition to dust samples from the SSD069 cruise, we also analyzed SRM987 and JNdi-1 standard reference material for $^{87}Sr/^{86}Sr$ and $^{143}Nd/^{144}Nd$, respectively, to ensure the quality of the data presented in this study. $^{87}Sr/^{86}Sr$ and $^{143}Nd/^{144}Nd$ measured in reference standards SRM987 and JNdi-1 yielded 0.710264 ± 0.000011; (1σ, n = 5) and 0.512105 ± 0.000009 (1σ, n = 6) respectively, agreeing well with the recommended values. An international rock standard (BCR-2) was also measured along with the aerosol samples, yielding $^{87}Sr/^{86}Sr$ and $^{143}Nd/^{144}Nd$ values of 0.705037 ± 0.000005 (1σ) and 0.512624 ± 0.000010 (1σ), which are consistent with certified reference values and literature reports (Table S1). The isotopic composition of Nd is often expressed as the deviation of $^{143}Nd/^{144}Nd$ in the dust samples relative to that of primitive chondrites and is commonly denoted as $\varepsilon_{Nd}(0)$, which is defined as follows.

$$\epsilon_{Nd}(0) = \left(\frac{\left({}^{143Nd}/_{144Nd} \right)_{Dust}}{\left({}^{143Nd}/_{144Nd} \right)_{CHUR}} - 1 \right) \times 10000$$

Here, CHUR refers to the Chondritic uniform reservoir and has a value of 0.512638 for the $^{143}Nd/^{144}Nd$ (Jacobsen and Wasserburg, 1980). The quartz filter substrates used for the collection of atmospheric dust over the Arabian Sea are strongly affected by the inherent relatively high filter blanks (Kumar et al., 2014). We, therefore, measured four quartz fibre filters (ca. 400 cm2) for ascertaining the blank levels of Sr and Nd (Table S2). However, the consistency in the isotopic composition and blank levels has allowed us to correct for the measured isotopic composition of Sr and Nd based on the mass balance equations. Another two filter blanks were processed for concentration of Sr (3.0-3.2 $ng.cm^{-2}$) and Nd (1.9-2.0 $ng.cm^{-2}$) as well as their isotopic ratios of $^{87}Sr/^{86}Sr$ (0.7147-0.7149) and $^{143}Nd/^{144}Nd$ (0.512433-0.512453). It is important to note that the Sr levels in the filter blanks are ~3 to 18% of the maximum and minimum signal observed in the dust samples collected over the Arabian Sea. Because of the rather low levels of Nd compared to Sr in dust samples, the measured signal of Nd in the filter blanks are only about 1.15 to 2 times that of the maximum and minimum levels observed for dust samples over the Arabian Sea during SSD069 cruise. Despite the high Nd levels in the blanks, the $\varepsilon_{Nd}(0)$ of the quartz filter blanks are characterized by a more positive values (i.e., ~ –3.9‰ more radiogenic than most of the sedimentary archives contributing to dust). Therefore, the following mass balance equations has been used to correct for procedural blanks and to assess the Sr and Nd isotopic composition of mineral dust collected over the Arabian Sea during SSD069/GI-10 expedition.

$$[Sr]_{total} = [Sr]_{true} + [Sr]_{blank} \qquad (1)$$

$$[Nd]_{total} = [Nd]_{true} + [Nd]_{blank} \qquad (2)$$

$$\left(\frac{^{87}Sr}{^{86}Sr}\right)_{total} = \frac{[Sr]_{true}}{[Sr]_{total}} \times \left(\frac{^{87}Sr}{^{86}Sr}\right)_{true} + \frac{[Sr]_{blank}}{[Sr]_{total}} \times \left(\frac{^{87}Sr}{^{86}Sr}\right)_{blank} \qquad (3)$$

$$(\varepsilon_{Nd}(0))_{total} = \frac{[Nd]_{true}}{[Nd]_{total}} \times (\varepsilon_{Nd}(0))_{true} + \frac{[Nd]_{blank}}{[Nd]_{total}} \times (\varepsilon_{Nd}(0))_{blank} \qquad (4)$$

2.3. Synoptic winds and air mass back trajectories

The prevailing regional meteorology over the deserts can provide hints on how the dust particles could be transported from several potential dust source areas (PDA) to the Arabian Sea in the winter season. For instance, earlier studies focusing on the synoptic winds over the Arabian Peninsula have suggested that dust transport from the deserts in the Middle East, which occurs mainly through the northeasterly winds (*aka. Shamals*; (Middleton, 1986; Pease et al., 1998; Aboobacker et al., 2021)). These *Shamals* are efficient transporters of dust particles to the Arabian Sea in winter and are likely triggered by southward movement of the persistent frontal depressions over alluvial basins between the Tigris - Euphrates (Al Ameri et al., 2019). However, the high-altitude convective upward and easterly progression of dust lofted from the Arabian Peninsula to the Arabian Sea in the winter season has also

been spotted by Tindale and Pease (1999). Considering these scenarios, we examined the synoptic winds at different vertical pressure levels (1000 mb: at the mean sea level; 700 mb: ~3 km above the mean sea level) to understand the dust transport to the Arabian Sea (Figure 2). Besides the wind patterns, air mass back trajectories (AMBTs) provide insights into how dust particles arrive over a receptor site. The AMBTs usually computed for 7-10 days using the Hybrid Single Particle Lagrangian Integrated Trajectory model (HYSPLIT, vers. 4.0; (Draxler, 2002; Stein et al., 2015)). Here, the HYSPLIT model uses the grided climatology data generated from a collaborative project between National Centers for Environmental Prediction (NCEP) and National Center for Atmospheric Research (NCAR) and is accessible from the web repository of the NOAA air resources laboratory (Figure 3).

2.4. Erodible dust fraction and dust optical properties

Dust emissions from the global land masses are a highly complex process and often depend on several parameters, including the soil erodibility (i.e., terrain roughness and soil moisture), dust load, the grain size of the dust (coarse or fine), and the columnar fraction of dust to total aerosols (Middleton, 1986; Prospero et al., 2002). Towards this, Ginoux et al. (2012) have constructed a map of erodible dust fraction per grid cell area based on the earlier soil erodibility related measurements from the PDA by combining with the satellite observation-based dust optical parameters (Figure 3). As such, the mineral aerosol load over a PDA can be obtained using the aerosol optical depth (AOD_{dust}: columnar loading of dust particles) retrievals from the Moderate Resolution Imaging Spectro Radiometer (MODIS) instrument, which is mounted onboard Aqua and Terra satellites (Hsu et al., 2004). Likewise, the relative size of the dust particles within a PDA can be obtained from the Deep blue algorithm based retrievals of dust angstrom exponent (AE_{dust}) values from the MODIS instrument (Hsu et al., 2006). We also estimated the mineral dust fraction (MDF), the ratio of dust aerosol extinction to total aerosol extinction retrieved at 550 nm, over the Arabian Sea based on the Modern Era Retrospective Regional Analysis (MERRA2) model (Gelaro et al., 2017; Veselovskii et al., 2018). Overall, we overlayed the 500 m AMBTs on the map of erodible dust fraction (Figure 3a), Deep blue algorithm-based MODIS retrievals of AOD and AE (Figure 3b, c), and the MERRA2 model based MDF (Figure 3d) over PDA surrounding the Arabian Sea during SSD069 cruise.

3. Results and discussion

3.1. Spatial variability of $^{87}Sr/^{86}Sr$ and $\varepsilon_{Nd}(0)$

$^{87}Sr/^{86}Sr$ and $\varepsilon_{Nd}(0)$ in the silicate fraction of mineral dust samples collected over the Arabian Sea during winter cruise (SSD069)/GI-10 have exhibited a marked spatial variability (Figure 4a,b). In particular, the dust samples collected over the west coast of India and the southern leg of the SSD069

track in the Arabian Sea were characterized by more radiogenic ^{87}Sr signal and, hence, had relatively high $^{87}Sr/^{86}Sr$ ratios than those dust samples collected over the pelagic waters. In contrast, we observed a more radiogenic ^{143}Nd signal and, hence, high $\varepsilon_{Nd}(0)$ for the pelagic dust samples compared to those collected alongside the coastal and southern Arabian Sea tracks of the SSD069 cruise. Several researchers have previously observed an inverse trend of Sr and Nd isotopic composition for the dust samples (Grousset and Biscaye, 2005; Turetta et al., 2016; Yan et al., 2020). Because the fact that Sr and Nd isotopic composition of dust particles aloft from the PDA are mostly governed by the surface lithology and are not affected by the weathering, long-range atmospheric transport, or biological processes (Grousset et al., 1992; Grousset and Biscaye, 2005), these tracers can be effectively used for the provenance studies. The source apportionment of dust particles over the Arabian Sea from this study can be achieved by understanding the possible PDA and thereby comparing the observed $^{87}Sr/^{86}Sr$ and $\varepsilon_{Nd}(0)$ signatures over this marine basin with the source profiles. One way to ascertain which PDA are utmost active and likely to contribute mineral aerosols during the SSD069 cruise is by examining the 7-day isentropic air mass back trajectories and synoptic wind patterns, which are described in the below sections.

3.3. Aeolian transport of dust, particle size, and absorption characteristics

The observed variations in the $^{87}Sr/^{86}Sr$ and $\varepsilon_{Nd}(0)$ of ambient aerosols collected over the Arabian Sea during the SSD069 cruise are mainly due to the differences in the provenance of mineral dust particles from which they have originated. To trace the probable source regions of mineral dust aerosols and associated transport pathways to the Arabian Sea from the neighboring land masses, we computed AMBTs at an arrival height of 500 m (i.e., close enough to typical boundary layer height in winter over South Asia) at the midpoints of the sampling tracks, similar to earlier studies (Siefert et al., 1999; Tindale and Pease, 1999; Kumar et al., 2020). The AMBT analysis has clearly hinted us the probable influence of mineral dust originating from the deserts in the Saudi Arabia, Iran, and India (Figure 3). Besides the AMBTs, the synoptic wind patterns at the mean sea level and at the height of ~3 km have clearly revealed that the northeasterly trade winds significantly influence the air over the Arabian Sea (Figure 2) (Badarinath et al., 2010; Aswini et al., 2020c). Several studies over the Indian Ocean during the winter season have successfully demonstrated the impact of atmospheric pollutants and fine alluvium from the Indo-Gangetic Plain over the Arabian Sea (Johansen and Hoffmann, 2004; Bikkina et al., 2012; Kumar et al., 2012; Aswini et al., 2020b; Bikkina et al., 2020). Therefore, we inferred that the dust samples collected over the Arabian Sea likely originated from northern India and the Middle East (i.e., Arabian Peninsula and Iran).

When we combine the Ginoux et al. (2012) data containing the fractional area of erodible dust per grid cell with AMBTs on a geographical map, this exercise has provided information about the relative significance of important dust source regions. These include four major locations (i) Saudi Arabia, (ii) Sistan basin and Lut Desert in Iran, (iii) alluvium from the IGP in northern India and Pakistan, and (iv) Peninsular India. Likewise, the satellite data on columnar loading of aerosols (AOD) at 550 nm revealed higher values over the IGP (i.e., ~0.6-1.0) and somewhat intermediate numbers observed over the desert regions in the Arabian Peninsula, Iran, Pakistan, and India (AOD: 0.4 – 0.6). This disparity is mainly because of the relatively high anthropogenic emissions (e.g., biomass/biofuel burning, vehicular exhaust, coal-fired thermal power plants) over the IGP together with the persistence of shallow atmospheric boundary layer in the winter season (i.e., vertical mixing of pollutants is, in general, confined to a certain height from the ground because of the insolation; ~700 m; (Nair et al., 2007)). Additionally, the aeolian transport of these trapped pollutants from the IGP sweeps out to the Arabian Sea through the prevailing NE monsoonal winds in winter. As a result, high AOD values were observed for the aerosol samples collected along the coastal track in the Arabian Sea of SSD069 cruise compared to those obtained over the pelagic waters due to the influence of continental transport from IGP (Figure 3b). Another important insight about the dust particle size over the different dust source regions can be traced from the angstrom exponent (AE) retrievals of dust based on the deep-blue algorithm (Hsu et al., 2006; Ginoux et al., 2012). The MODIS deep-blue product of dust AE values are lower over the desert regions of the Arabian Peninsula compared to other deserts in the Middle East and India during the SSD069 cruise. This result implies that the mineral dust particles over the deserts of the Arabian Peninsula are much coarser than those originating from Iran, Pakistan, and India during the study period (Figure 3c). Likewise, we can also understand the relative importance of dust emissions among different source regions, given the influence of long-range transport of other particulate components in the air using the estimated mineral dust fraction (MDF). Here, MDF (as explained in methods) refers to light extinction caused by the dust particles normalized to that of total particles suspended in the ambient air column at 550 nm (Francis et al., 2022; Gkikas et al., 2022). This MDF is computed based on the spatial maps of AOD_{dust} and AOD_{total}, obtained from the MERRA-2 datasets. By and large, we observed higher MDF values over the Arabian Peninsula compared to other deserts of Iran, Pakistan, and India (Figure 3d). This means dust emissions from the Arabian Peninsula are more likely to influence the Arabian Sea compared to other dust source regions in the Middle East and India.

3.4. Dust Storms – influence from Saudi Arabia and Iran

Based on the satellite remote sensing products, for instance, aerosol index data from the Total Ozone Mapping Spectrometer (TOMS), Prospero and other peers have pointed out that the intensity of dust emissions usually peaks during summer months and dust transport to the AS is mainly occur through the high-altitude transport (Middleton, 1986; Prospero et al., 2002; Rashki et al., 2021). This is because of the strong SW monsoonal surface winds that blew off alongside the Somali, and Oman coast towards the Indian subcontinent (i.e., a phenomenon commonly referred as "*Somali jet* or *Findlater Jet*") prevents the intrusion of dust particles at the ground level from Arabian Peninsula to the Arabian Sea. Nevertheless, Middleton (1986) had argued that dust outbreaks from the horn of Africa (Somali coast) to the Arabian Sea mostly contribute to the aeolian dust during summer (June-September), inferred from the dust frequency and associated distribution/visibility data maps (storms <1km; blowing dust: <11 km),). Likewise, recent studies have highlighted that the Sistan basin in southeastern Iran is also an active PDA, contributing immensely to the dispersal of aeolian dust over the northern Arabian Sea during summer season (June-September) ((Kaskaoutis et al., 2014; Rashki et al., 2021; Mohammadpour et al., 2022). Contrary to conventional vision, the dust storms triggered by *Levar* and *Shamal* winds are not only specific to summer months but also frequently occur during other seasons. The National Aeronautics and Space Administration (NASA) has initiated the tracking of dust plumes over the Indian Ocean using the Earth-orbiting satellites, and the related snapshot imagery of dust storm outbreaks over the Arabian Sea was archived in public databases of Earth Observing System Data and Information System (EOSDIS; Ramapriyan et al., 2010).

To illustrate the importance of dust outbreaks from the Arabian Peninsula and Iran region, some of the EOSDIS were randomly picked and provided in the supplementary information (Figure S1). These EOSDIS archived repository images have highlighted the influence of dust outbreaks from the Iran in December 2004, January 2012, February 2016, and January 2022. Using the EOSDIS database, we also looked for any such occurrence of dust storm events and the subsequent impact on the Arabian Sea during the SSD069 cruise. A close analysis of the dust storm images obtained from the MODIS archived datasets (https://worldview.earthdata.nasa.gov/) have hinted us the possible influence of two such events during SSD069 cruise. One dust storm originated from Saudi Arabia by Shamal winds on 27 January 2020 (Figure 5a), and another originated from Iran by *Levar* winds on 10 February 2020 (Figure 5b). However, no such dust storms were observed from the horn of Africa. This means, the observed Sr and Nd isotopic composition of mineral dust on 27 January 2020 over the Arabian Sea is likely a source-specific signature of *Shamal* wind-fuelled dust event. In contrast, the $^{87}Sr/^{86}Sr$ and $\varepsilon_{Nd}(0)$ of DS2 is somewhat in close resemblance with the mineral aerosol emissions from

Iran region. Recently, Kumar et al. (2020) have documented the impact of dust plumes from Iran in summer months based on the Sr and Nd isotopic composition of ambient aerosols from a coastal urban site, Goa (India). However, such emphasis on wintertime dust storms over the Arabian Sea is still lacking in the literature. Therefore, the DS2 image from 10th February 2020 (i.e., the Suomi National Polar-orbiting Partnership Visible Infrared Imaging Radiometer Suite (NPP-VIIRS) true colour image of the dust storm event obtained from the EOSDIS web repository, Figure 5b) together with the AMBTs further revealed an influence from the Iran region. Subsequently, we have tagged the $^{87}Sr/^{86}Sr$ and $\varepsilon_{Nd}(0)$ of DS1 and DS2 with their probable source regions and compared these isotopic tracer data with the source profile data documented in the literature (Blanchet, 2019; Jewell et al., 2021; Robinson et al., 2021; Kunkelova et al., 2022).

3.5. Difference(s) in the lithology of the dust source

The lithology of Saudi Arabia and the neighbouring deserts differ greatly from the arid soils present in Iran, Afghanistan, Pakistan, and India (Pease et al., 1998; Tindale and Pease, 1999). Consequently, the geographical variability in the source-specific Sr and Nd isotopic composition of these soils are intricately coupled with their formation history. For instance, dust originating from the older rocks (*e.g.*, Australia; (Delmonte et al., 2004; Revel-Rolland et al., 2006)) are characterized by more $^{87}Sr/^{86}Sr$ (>0.715) and less $\varepsilon_{Nd}(0)$ (-11 to -21) than the juvenile bedrock lithology of island arcs of Indonesia (i.e., containing relatively low $^{87}Sr/^{86}Sr$ ratios (~0.709) and more $\varepsilon_{Nd}(0)$ (Whitford, 1975; Vroon et al., 1993). Likewise, the mineral dust originating from the Thar Desert in Rajasthan (Yadav and Rajamani, 2004) are characterized by higher and lower values of $^{87}Sr/^{86}Sr$ and $\varepsilon_{Nd}(0)$, respectively compared to those documented for the Arabian Peninsula and Iran (Robinson et al., 2021; Kunkelova et al., 2022). However, the Sr and Nd isotopic composition of Thar dust is in sharp contrast to those observed for the fine alluvium of the Indo-Gangetic Plain and other nearby arid regions of Middle East (Yadav and Rajamani, 2004; Tripathi et al., 2013; Kumar et al., 2020). Taken together, therefore, dust particles originating from these PDA of different lithology could contribute to significant variability in the observed Sr and Nd isotopic signatures. As such understanding, the differences in the lithology of the deserts bordering the Arabian Sea could provide some hint on the persisting variability of Sr and Nd isotopic composition of the different provenance(s). Therefore, the 500m AMBTs were overlapped on the simplified geology map (Figure 6) compiled by the Canadian GIS group (Chorlton, 2007). Furthermore, we also compared spatial variability data of $^{87}Sr/^{86}Sr$ and $\varepsilon_{Nd}(0)$ with those signatures of PDA on a geographical map containing the AMBTs (Figure 7).

3.5. Source apportionment

The Sr-Nd isotopic composition of mineral aerosols collected over the Arabian Sea is highly dependent on the contributing dust particles from the surrounding deserts/alluvial plains in the Middle East and South Asia (Jewell et al., 2021; Kunkelova et al., 2022). Despite having a large variability in the $^{87}Sr/^{86}Sr$ and $\varepsilon_{Nd}(0)$ of these surface soils (Goldstein et al., 1984; Goldstein and Jacobsen, 1988; Grousset and Biscaye, 2005; Liégeois and Stern, 2010; Muhs et al., 2014; Robinson et al., 2021), the overlying dust in the ambient air carries more or less similar signature specific to these potential dust-source areas (PDA)(Goldstein and Jacobsen, 1988). The PDA bordering the Arabian Sea include the arid/semiarid regions in Somalia, Yemen, Oman, Saudi Arabia (e.g., Rub-Al-Khali, An-Nefud, Dahna), Iraq, Iran (Sistan basin), Afghanistan, Pakistan, and India (Thar). Furthermore, the back trajectories of most of the west coast sampling locations and the south-eastern Arabian Sea traverse over southern Peninsular India, influenced by the terrain lithology of the Peninsular Gneissic Complex (PGC). All these geographical domains are characterized by a distinct pair of Sr-Nd isotopic composition mainly because of their lithology, which depends on the formation history of the respective basin (Muhs et al., 2014; Jewell et al., 2021; Robinson et al., 2021; Suresh et al., 2021; Kunkelova et al., 2022).

Numerous studies have shown distinct $^{87}Sr/^{86}Sr$ and $\varepsilon_{Nd}(0)$ values for the PDA in the Middle East and South Asia (Sirocko, 1994; Jewell et al., 2021; Suresh et al., 2021; Kunkelova et al., 2022)). Earlier Sirocko (1994) had reported a $^{87}Sr/^{86}Sr$ and $\varepsilon_{Nd}(0)$ values of 0.7091 and -6, respectively for the aeolian dust transported to the Arabian Sea. Likewise, the updated compilation of Kunkelova et al. (2022) has shown that aeolian dust from the Arabian Peninsula is characterized by a distinct pair of $^{87}Sr/^{86}Sr$ (0.7115±0.0012) and $\varepsilon_{Nd}(0)$ (-6.4±1.8) values, which are in sharp contrast to those observed for the soils of eastern Sahara ($^{87}Sr/^{86}Sr$:0.7059±0.0017 and $\varepsilon_{Nd}(0)$ (-1.1±2.7), Jewell et al. (2021)). Kumar et al. (2020) have characterized aeolian dust signatures of $^{87}Sr/^{86}Sr$ (0.7109-0.7135) and $\varepsilon_{Nd}(0)$ (-7.8 to -5.4) from Iran (mostly originated from Sistan basin and Makran coast) to the Arabian Sea. Furthermore, Singh et al. (2008) have shown that alluvial soils of the Indo-Gangetic Plain are characterized by higher $^{87}Sr/^{86}Sr$ ratios (0.7527-0.7893) and lower $\varepsilon_{Nd}(0)$ (-18.6 to -15.7) than those reported for the deserts in the Middle East (Kumar et al., 2020; Jewell et al., 2021; Kunkelova et al., 2022) and Thar ($^{87}Sr/^{86}Sr$: 0.7290-0.390; $\varepsilon_{Nd}(0)$: -15.9 to -12.6; (Yadav and Rajamani, 2004)). Therefore, we have compared our Sr and Nd isotopic composition data of the SSD069 cruise in the Arabian Sea with the available data from these PDAs (Figure 8).

Studies focussing on the relative significance of mineral aerosol emissions from different PDA to the Arabian Sea based on $^{87}Sr/^{86}Sr$ and $\varepsilon_{Nd}(0)$ have been so far conducted from a coastal urban site (Goa) in southwestern India (Kumar et al., 2020; Suresh et al., 2021). More specifically, these studies have tagged different dust events, mostly from summer months (June-September; (Kumar et al., 2020); plotted in in Figure 8) and few dust samples from before and after the onset of SW monsoon (Suresh et al., 2021). In contrast, our data on $^{87}Sr/^{86}Sr$ and $\varepsilon_{Nd}(0)$ is based on the atmospheric dust samples collected over the Arabian Sea in winter season. We have, therefore compared these two data sets to gain insights on seasonal differences in the provenance of mineral dust and their aeolian routes to the Arabian Sea (Figure 8).

Among all, the dust samples collected from the MABL alongside the west coast of peninsular India are characterized by higher $^{87}Sr/^{86}Sr$ ratios and lower $\varepsilon_{Nd}(0)$ values than those from open ocean waters of the Arabian Sea. These data are consistent with the $^{87}Sr/^{86}Sr$ ratios reported for Thar soils, however, are not overlapping with the reported ranges for $\varepsilon_{Nd}(0)$. AMBT analysis shows that southern Peninsular India, partly the Lesser Himalaya (LH) and the IGP could also be possible contributors of mineral aerosols over the Arabian Sea in the winter season. Ahmad et al. (2000) have reported that the lithology of the Lesser Himalaya is characterized by a broad range for $^{87}Sr/^{86}Sr$ (0.7158-1.1765) and $\varepsilon_{Nd}(0)$ values (-27.7 to -15.0). Likewise, numerous studies have documented that fluvial sediments and source rocks of the IGP are highly radiogenic for Sr ($^{87}Sr/^{86}Sr$: 0.72 – 0.83; (Singh et al., 2008; Tripathy et al., 2011; Tripathi et al., 2013; Awasthi et al., 2018)). In contrast, the soil particles of PGC are characterized by both relatively low $^{87}Sr/^{86}Sr$ (0.71507 – 0.72176) and low $\varepsilon_{Nd}(0)$ values (-40.8 to -32.6; (Goswami et al., 2012)). However, subsequent studies have reported a rather diverse range of Sr and Nd isotopic composition with mean values of 0.7344 for $^{87}Sr/^{86}Sr$ and $\varepsilon_{Nd}(0)$ (-23.6) for the PGC dataset (Yu et al., 2019)). The impact of PGC dust in terms of high Mn supply has been projected recently for both aerosols originating from southern India (Aswini et al., 2020a) and for the surface seawater data (Singh et al., 2023). In contrast, the tracer pair of Sr and Nd signals for the remaining dust samples collected over the pelagic waters of the Arabian Sea were remarkably overlapped with the recent source profile data from the Arabian Peninsula/Iran (Palchan et al., 2013; Robinson et al., 2021; Kunkelova et al., 2022). Therefore, we have pinpointed the probable source region(s) of aeolian dust over the Arabian Sea are the Arabian Peninsula/Iran versus the IGP/PGC by comparing their Sr and Nd isotope composition (Figure 8). Furthermore, $^{87}Sr/^{86}Sr$ and $\varepsilon_{Nd}(0)$ of dust samples reported from Goa (Kumar et al., 2020) are compared with this study in Figure 8 to highlight the seasonal differences in the source regions of mineral dust (if any).

Kumar et al. (2020) have characterized three different types of dust particles collected over Goa using $^{87}Sr/^{86}Sr$ and $\varepsilon_{Nd}(0)$, and traced back their origin from Arabian Peninsula (ARBS: 0.7125-0.7142; -7.8 to -7.3), Iran (SWAS: 0.7143-0.7206; -20.1 to -7.4), and Thar (SWAW:0.7052-0.7148; -12.8 to -8.3) using the AMBTs. Interestingly, the $^{87}Sr/^{86}Sr$ ratios of dust sampled over the open ocean waters during SSD069 cruise are consistent with those reported for ARBS, source-emissions from Arabian Peninsula (0.7115, (Kunkelova et al., 2022); 0.709, (Sirocko, 1994)). However, $\varepsilon_{Nd}(0)$ values for pelagic dust samples collected over the Arabian Sea during SSD069 cruise (-13.7 to -9.3) were lower than those documented over Goa by (ARBS: -7.8 to -7.3; Kumar et al., 2020) and the source emissions (-6.4±1.8, (Kunkelova et al., 2022); -6, (Sirocko, 1994)). This means observed signatures over the pelagic waters of the Arabian Sea during our winter cruise could likely be due to the mixture of dust particles from the Arabian Peninsula with other dust source-emissions in South Asia, which contain lower $\varepsilon_{Nd}(0)$ and higher $^{87}Sr/^{86}Sr$ ratios (viz., Thar, PGC, IGP; Table 2).

Of these, dust particles from the Thar are characterized by slightly higher $^{87}Sr/^{86}Sr$ ratios and lower $\varepsilon_{Nd}(0)$ values (0.7289-0.7390 and -15.9 to -12.6, respectively) than those reported for the deserts in the Middle East (Table 2, Tripathi et al., 2013). In contrast, the PGC and IGP end members are characterized by somewhat higher $^{87}Sr/^{86}Sr$ ratios (~0.72 and 0.73-0.80) and lower $\varepsilon_{Nd}(0)$ values ((-25 to -20; -20 to -15, ((Singh et al., 2008; Tripathi et al., 2013; Awasthi et al., 2018; Yu et al., 2019)). As apparent from the Sr-Nd isotopic signatures of these end members, we suggest that dust samples collected over the open ocean waters are mostly derived from Arabian Peninsula and Thar since the MABL during the SSD069 cruise is strongly influenced by the prevailing NE monsoonal winds. We, therefore, used a two-end member mixing of source emissions to constrain the overall relative contribution of mineral dust from each provenance (Arabian Peninsula or AP: ~80-90%; Thar: ~10-20%).

$$\left(\frac{^{87}Sr}{^{86}Sr}\right)_{mix} = \frac{f_{dust-AP} \times [Sr]_{AP} \times \left(\frac{^{87}Sr}{^{86}Sr}\right)_{dust-AP} + (1 - f_{dust-AP}) \times [Sr]_{Thar} \times \left(\frac{^{87}Sr}{^{86}Sr}\right)_{dust-Thar}}{f_{dust-AP} \times [Sr]_{AP} + (1 - f_{dust-AP}) \times [Sr]_{Thar}}$$

$$(\varepsilon_{Nd}(0))_{mix} = \frac{f_{dust-AP} \times [Nd]_{AP} \times (\varepsilon_{Nd}(0))_{dust-AP} + (1 - f_{dust-AP}) \times [Nd]_{Thar} \times (\varepsilon_{Nd}(0))_{dust-Thar}}{f_{dust-AP} \times [Nd]_{AP} + (1 - f_{dust-AP}) \times [Nd]_{Thar}}$$

Here, we adopted the concentrations and isotopic composition of Sr (AP: 0.708; Thar: 0.735) and Nd (AP: -7; Thar: -13.5) for the source-emissions from (Kumar et al., 2020). Similar to these above calculations, the remaining dust samples collected along the west coast of India could be explained by two-end member mixing of the source emissions from the PGC (80-90%) and Arabian Peninsula (~10-20%).

It is important to reiterate the possible bias in the source estimation which could arise from the grain size sorting effect during long-range atmospheric transport while using the observed isotope composition of Sr and Nd of dust particles over the Arabian Sea with the source-emissions in the Middle East and South Asia. Several studies have shown that $\varepsilon_{Nd}(0)$ signatures of detrital silicates in the distal locations remain similar to that of source-emissions from PDA ((Goldstein et al., 1984; Grousset et al., 1988; Kanayama et al., 2005; Meyer et al., 2011). However, grain size sorting, (i.e., due to relative increase in contribution of clay fraction which contains more radiogenic Sr character compared to sand/silt fraction) might influence the observed $^{87}Sr/^{86}Sr$ ratios during transport (Blum and Erel, 2003; Meyer et al., 2011). However, the associated variability (increase) of $^{87}Sr/^{86}Sr$ ratios with a decrease in particle size within the source emissions of PDA in the Middle East is not obvious from the recent compilation of Kunkelova et al. (2022). A large data set will be required to constrain such secondary effects during transport which is beyond the scope of this study. Moreover, Duce et al., 1991 have pointed out that only particles smaller than 10 μm are usually involved in long-range transport away from the dust source regions. Consequently, the measured isotopic composition of Sr and Nd of dust particles collected over the Arabian Sea is likely because of small-size silt and clay particles. Considering the inferences from the available field data that the Nd-isotopic composition could serve as a robust proxy for source apportionment of mineral dust, we, therefore, used the large variabilities observed in $\varepsilon_{Nd}(0)$ values that are coherent with $^{87}Sr/^{86}Sr$ to characterize the influence of different dust source regions. We could observe a clear distinction of $\varepsilon_{Nd}(0)$ between the open ocean dust samples (Dust#08-13) compared to those collected alongside the East coast of the Arabian Sea.

As mentioned earlier, we encountered two dust storms over the Arabian Sea, DS1 was from Arabian Peninsula on 27 January 2020 and DS2 was from Iran on 10 February 2020. The $^{87}Sr/^{86}Sr$ and $\varepsilon_{Nd}(0)$ values during DS1 (i.e., Dust#08) and DS2 were not only consistent with the other four dust samples (Dust#09-12) collected over the open ocean waters of the Arabian Sea but also compared well with the source profile of mineral aerosols from Saudi Arabia (Figure 8). Furthermore, as indicated earlier, the AMBTs for all these six dust samples (including the DS1, 2) have origins from the Middle East deserts. This observation is perhaps related to the source-specific dust influence of dust storms originating from the Saudi Arabia and other nearby deserts in the Middle East during winter season. Besides, the $^{87}Sr/^{86}Sr$ and $\varepsilon_{Nd}(0)$ signatures for the dust samples collected along west coast of India are rather diverse and possibly could be from a mixture of source emissions in Iran, Afghanistan, Pakistan, and India. Overall, our results clearly emphasized the importance of dust supply from Saudi Arabia and Iran regions to the Arabian Sea during the winter season.

4. Conclusions

This study first time attempts to examine the ship-borne collection of dust samples over the Arabian Sea during a winter cruise to characterize the provenance(s) based on the $^{87}Sr/^{86}Sr$ and $\varepsilon_{Nd}(0)$. We also used AMBTs, wind patterns, and earth-orbiting satellite (EOS) based retrievals of dust optical properties to further understand the nature of dust particles (coarse vs. fine nature) transported to the Arabian Sea and which potential dust source areas are more likely to contribute in terms of emissions during the winter season. Our results based on the Sr and Nd isotopic composition of detrital silicate fraction of ambient aerosols have shed light on the importance of dust outbreaks from the Arabian Peninsula and Iran during winter cruise, otherwise not conceived in terms of general synoptic scale transport impact of haze pollution from South Asia. Sr-Nd isotope signatures along with AMBTs of the dust particles suggest the Arabian Peninsula/Iran as the major source of dust to the open ocean of the Arabian Sea whereas the eastern Arabian Sea receives mineral dust mostly from the Peninsular India and the Indo-Gangetic Plain in winter months.

Acknowledgments

We thank the Chief scientist and Ship captain/crew for the logistic support onboard SSD069. SB acknowledges the funding support from SERB-Ramanujan Fellowship (RJF/2020/000036). Analyses and visualizations used in this [study/paper/presentation] were produced with the Giovanni online data system, developed, and maintained by the NASA GES DISC. The authors gratefully acknowledge the NOAA Air Resources Laboratory (ARL) for the provision of the HYSPLIT transport and dispersion model and/or READY website (https://www.ready.noaa.gov)

used in this publication. We thank both reviewers and Editor for their constructive comments and suggestions during the review process.

Author contributions

SB: Writing the original draft and sample preparation for trace elements and isotopic (Sr and Nd) measurements in the Clean-lab facility of NIO; AS: column chromatography and Sr-Nd isotopic composition measurements on MC-ICP-MS at CSIR-NIO; DK: assisted in the extraction of samples; NDS and BS: collected dust samples; SKS: Conceived the project, acquired funding, actively involved in supervising the analysis, data quality, and revising the manuscript.

References

Aboobacker VM, Samiksha SV, Veerasingam S, Al-Ansari EMAS, Vethamony P. Role of shamal and easterly winds on the wave characteristics off Qatar, central Arabian Gulf. Ocean Engineering 2021; 236: 109457.

Ahmad T, Harris N, Bickle M, Chapman H, Bunbury J, Prince C. Isotopic constraints on the structural relationships between the Lesser Himalayan Series and the High Himalayan Crystalline Series, Garhwal Himalaya. GSA Bulletin 2000; 112: 467-477.

Al Ameri IDS, Briant RM, Engels S. Drought severity and increased dust storm frequency in the Middle East: a case study from the Tigris–Euphrates alluvial plain, central Iraq. Weather 2019; 74: 416-426.

Aswini A, Hegde P, Aryasree S, Girach IA, Nair PR. Continental outflow of anthropogenic aerosols over Arabian Sea and Indian Ocean during wintertime: ICARB-2018 campaign. Science of the Total Environment 2020a; 712: 135214.

Aswini AR, Hegde P, Aryasree S, Girach IA, Nair PR. Continental outflow of anthropogenic aerosols over Arabian Sea and Indian Ocean during wintertime: ICARB-2018 campaign. Science of The Total Environment 2020b; 712: 135214.

Aswini M, Kumar A, Das SK. Quantification of long-range transported aeolian dust towards the Indian peninsular region using satellite and ground-based data-A case study during a dust storm over the Arabian Sea. Atmospheric Research 2020c; 239: 104910.

Awasthi N, Ray E, Paul D. Sr and Nd isotope compositions of alluvial sediments from the Ganga Basin and their use as potential proxies for source identification and apportionment. Chemical Geology 2018; 476: 327-339.

Badarinath KVS, Kharol SK, Kaskaoutis DG, Sharma AR, Ramaswamy V, Kambezidis HD. Long-range transport of dust aerosols over the Arabian Sea and Indian region — A case study using satellite data and ground-based measurements. Global and Planetary Change 2010; 72: 164-181.

Banerjee P, Kumar SP. ENSO modulation of interannual variability of dust aerosols over the northwest Indian Ocean. Journal of Climate 2016; 29: 1287-1303.

Banerjee P, Prasanna Kumar S. Dust-induced episodic phytoplankton blooms in the Arabian Sea during winter monsoon. Journal of Geophysical Research: Oceans 2014; 119: 7123-7138.

Basu S, Gledhill M, de Beer D, Prabhu Matondkar SG, Shaked Y. Colonies of marine cyanobacteria Trichodesmium interact with associated bacteria to acquire iron from dust. Communications Biology 2019; 2: 284.

Bikkina P, Sarma VVSS, Kawamura K, Bikkina S, Kunwar B, Sherin CK. Chemical characterization of wintertime marine aerosols over the Arabian Sea: Impact of marine sources and long-range transport. Atmospheric Environment 2020: 117749.

Bikkina S, Sarin M. Atmospheric pathways of phosphorous to the Bay of Bengal: contribution from anthropogenic sources and mineral dust. Tellus B 2012; 64.

Bikkina S, Sarin M, Kumar A. Impact of anthropogenic sources on aerosol iron solubility over the Bay of Bengal and the Arabian Sea. Biogeochemistry 2012; 110: 257-268.

Blanchet CL. A database of marine and terrestrial radiogenic Nd and Sr isotopes for tracing earth-surface processes. Earth Syst. Sci. Data 2019; 11: 741-759.

Blum JD, Erel Y. Radiogenic isotopes in weathering and hydrology. Treatise on geochemistry 2003; 5: 605.

Choobari OA, Zawar-Reza P, Sturman A. The global distribution of mineral dust and its impacts on the climate system: A review. Atmospheric Research 2014; 138: 152-165.

Chorlton LB. Generalized geology of the world: bedrock domains and major faults in GIS format: a small-scale world geology map with an extended geological attribute database. Geological Survey of Canada, Open File 5529, 2007, 48 pages; 2007: 48, doi: 10.4095/223767.

Delmonte B, Basile-Doelsch I, Petit J-R, Maggi V, Revel-Rolland M, Michard A, et al. Comparing the Epica and Vostok dust records during the last 220,000 years: stratigraphical correlation and provenance in glacial periods. Earth-Science Reviews 2004; 66: 63-87.

Draxler RR. Forecasting dust storms using Hysplit. Proceedings of Sino-US Workshop on Dust Storms and Their Effects on Human Health, November, 2002, pp. 25-26.

Duce RA, Liss PS, Merrill JT, Atlas EL, Buat-Menard P, Hicks BB, et al. The atmospheric input of trace species to the world ocean. Global Biogeochemical Cycles 1991; 5: 193-259.

Francis D, Fonseca R, Nelli N, Teixido O, Mohamed R, Perry R. Increased Shamal winds and dust activity over the Arabian Peninsula during the COVID-19 lockdown period in 2020. Aeolian Research 2022; 55: 100786.

Gelaro R, McCarty W, Suárez MJ, Todling R, Molod A, Takacs L, et al. The modern-era retrospective analysis for research and applications, version 2 (MERRA-2). Journal of climate 2017; 30: 5419-5454.

Ginoux P, Prospero JM, Gill TE, Hsu NC, Zhao M. Global-scale attribution of anthropogenic and natural dust sources and their emission rates based on MODIS Deep Blue aerosol products. Reviews of Geophysics 2012; 50.

Gkikas A, Proestakis E, Amiridis V, Kazadzis S, Di Tomaso E, Marinou E, et al. Quantification of the dust optical depth across spatiotemporal scales with the MIDAS global dataset (2003–2017). Atmos. Chem. Phys. 2022; 22: 3553-3578.

Goldstein SJ, Jacobsen SB. Nd and Sr isotopic systematics of river water suspended material: implications for crustal evolution. Earth and Planetary Science Letters 1988; 87: 249-265.

Goldstein SL, O'Nions RK, Hamilton PJ. A Sm-Nd isotopic study of atmospheric dusts and particulates from major river systems. Earth and Planetary Science Letters 1984; 70: 221-236.

Goswami V, Singh SK, Bhushan R, Rai VK. Temporal variations in 87Sr/86Sr and εNd in sediments of the southeastern Arabian Sea: Impact of monsoon and surface water circulation. Geochemistry, Geophysics, Geosystems 2012; 13.

Grousset FE, Biscaye PE. Tracing dust sources and transport patterns using Sr, Nd and Pb isotopes. Chemical Geology 2005; 222: 149-167.

Grousset FE, Biscaye PE, Zindler A, Prospero J, Chester R. Neodymium isotopes as tracers in marine sediments and aerosols: North Atlantic. Earth and Planetary Science Letters 1988; 87: 367-378.

Grousset FE, Rognon P, Coudé-Gaussen G, Pédemay P. Origins of peri-Saharan dust deposits traced by their Nd and Sr isotopic composition. Palaeogeography, Palaeoclimatology, Palaeoecology 1992; 93: 203-212.

Guieu C, Al Azhar M, Aumont O, Mahowald N, Levy M, Ethé C, et al. Major Impact of Dust Deposition on the Productivity of the Arabian Sea. Geophysical Research Letters 2019; 46: 6736-6744.

Hsu NC, Tsay S-C, King MD, Herman JR. Aerosol properties over bright-reflecting source regions. IEEE transactions on geoscience and remote sensing 2004; 42: 557-569.

Hsu NC, Tsay S-C, King MD, Herman JR. Deep blue retrievals of Asian aerosol properties during ACE-Asia. IEEE transactions on geoscience and remote sensing 2006; 44: 3180-3195.

Ito T, Nenes A, Johnson MS, Meskhidze N, Deutsch C. Acceleration of oxygen decline in the tropical Pacific over the past decades by aerosol pollutants. Nature Geoscience 2016; 9: 443-447.

Jacobsen SB, Wasserburg G. Sm-Nd isotopic evolution of chondrites. Earth and Planetary Science Letters 1980; 50: 139-155.

Jewell AM, Drake N, Crocker AJ, Bakker NL, Kunkelova T, Bristow CS, et al. Three North African dust source areas and their geochemical fingerprint. Earth and Planetary Science Letters 2021; 554: 116645.

Jickells T, An Z, Andersen KK, Baker A, Bergametti G, Brooks N, et al. Global iron connections between desert dust, ocean biogeochemistry, and climate. Science 2005; 308: 67-71.

Jickells T, Boyd P, Hunter KA. Biogeochemical impacts of dust on the global carbon cycle. Mineral Dust. Springer, 2014, pp. 359-384.

Johansen AM, Hoffmann MR. Chemical characterization of ambient aerosol collected during the northeast monsoon season over the Arabian Sea: Anions and cations. Journal of Geophysical Research: Atmospheres 2004; 109.

Kanayama S, Yabuki S, Zeng F, Liu M, Shen Z, Liu L, et al. Size-Dependent Geochemical Characteristics of Asian Dust—Sr and Nd Isotope Compositions as Tracers for Source Identification—. Journal of the Meteorological Society of Japan. Ser. II 2005; 83: 107-120.

Kaskaoutis DG, Rashki A, Houssos EE, Goto D, Nastos PT. Extremely high aerosol loading over Arabian Sea during June 2008: The specific role of the atmospheric dynamics and Sistan dust storms. Atmospheric Environment 2014; 94: 374-384.

Keith Moore J, Doney SC, Lindsay K, Mahowald N, Michaels AF. Nitrogen fixation amplifies the ocean biogeochemical response to decadal timescale variations in mineral dust deposition. Tellus B: Chemical and Physical Meteorology 2006; 58: 560-572.

Kumar A, Abouchami W, Galer SJG, Garrison VH, Williams E, Andreae MO. A radiogenic isotope tracer study of transatlantic dust transport from Africa to the Caribbean. Atmospheric Environment 2014; 82: 130-143.

Kumar A, Sarin MM, Sudheer AK. Mineral and anthropogenic aerosols in Arabian Sea–atmospheric boundary layer: Sources and spatial variability. Atmospheric Environment 2008; 42: 5169-5181.

Kumar A, Sudheer AK, Goswami V, Bhushan R. Influence of continental outflow on aerosol chemical characteristics over the Arabian Sea during winter. Atmospheric Environment 2012; 50: 182-191.

Kumar A, Suresh K, Rahaman W. Geochemical characterization of modern aeolian dust over the Northeastern Arabian Sea: Implication for dust transport in the Arabian Sea. Science of The Total Environment 2020; 729: 138576.

Kunkelova T, Crocker AJ, Jewell AM, Breeze PS, Drake NA, Cooper MJ, et al. Dust sources in Westernmost Asia have a different geochemical fingerprint to those in the Sahara. Quaternary Science Reviews 2022; 294: 107717.

Liégeois J-P, Stern RJ. Sr–Nd isotopes and geochemistry of granite-gneiss complexes from the Meatiq and Hafafit domes, Eastern Desert, Egypt: No evidence for pre-Neoproterozoic crust. Journal of African Earth Sciences 2010; 57: 31-40.

Lightfoot PC, Hawkesworth CJ, Devey CW, Rogers NW, Calsteren PWCV. Source and Differentiation of Deccan Trap Lavas: Implications of Geochemical and Mineral Chemical Variations. Journal of Petrology 1990; 31: 1165-1200.

Madhupratap M, Kumar SP, Bhattathiri PMA, Kumar MD, Raghukumar S, Nair KKC, et al. Mechanism of the biological response to winter cooling in the northeastern Arabian Sea. Nature 1996; 384: 549-552.

Mahowald NM, Scanza R, Brahney J, Goodale CL, Hess PG, Moore JK, et al. Aerosol Deposition Impacts on Land and Ocean Carbon Cycles. Current Climate Change Reports 2017: 1-16.

Meyer I, Davies GR, Stuut J-BW. Grain size control on Sr-Nd isotope provenance studies and impact on paleoclimate reconstructions: An example from deep-sea sediments offshore NW Africa. Geochemistry, Geophysics, Geosystems 2011; 12.

Middleton NJ. Dust storms in the Middle East. Journal of Arid Environments 1986; 10: 83-96.

Mohammadpour K, Rashki A, Sciortino M, Kaskaoutis DG, Darvishi Boloorani A. A statistical approach for identification of dust-AOD hotspots climatology and clustering of dust regimes over Southwest Asia and the Arabian Sea. Atmospheric Pollution Research 2022; 13: 101395.

Muhs DR, Prospero JM, Baddock MC, Gill TE. Identifying sources of aeolian mineral dust: Present and past. Mineral dust. Springer, 2014, pp. 51-74.

Nair VS, Moorthy KK, Alappattu DP, Kunhikrishnan P, George S, Nair PR, et al. Wintertime aerosol characteristics over the Indo-Gangetic Plain (IGP): Impacts of local boundary layer processes and long-range transport. Journal of Geophysical Research: Atmospheres (1984–2012) 2007; 112: doi: 10.1029/2006JD008099.

Pabortsava K, Lampitt RS, Benson J, Crowe C, McLachlan R, Le Moigne FAC, et al. Carbon sequestration in the deep Atlantic enhanced by Saharan dust. Nature Geoscience 2017; 10: 189-194.

Palchan D, Stein M, Almogi-Labin A, Erel Y, Goldstein SL. Dust transport and synoptic conditions over the Sahara–Arabia deserts during the MIS6/5 and 2/1 transitions from grain-size, chemical and isotopic properties of Red Sea cores. Earth and Planetary Science Letters 2013; 382: 125-139.

Patra PK, Kumar MD, Mahowald N, Sarma VVSS. Atmospheric deposition and surface stratification as controls of contrasting chlorophyll abundance in the North Indian Ocean. Journal of Geophysical Research: Oceans 2007; 112.

Pease PP, Tchakerian VP, Tindale NW. Aerosols over the Arabian Sea: geochemistry and source areas for aeolian desert dust. Journal of Arid Environments 1998; 39: 477-496.

Prospero JM, Ginoux P, Torres O, Nicholson SE, Gill TE. Environmental characterization of global sources of atmospheric soil dust identified with the Nimbus 7 Total Ozone Mapping Spectrometer (TOMS) absorbing aerosol product. Reviews of geophysics 2002; 40.

Ramapriyan HK, Behnke J, Sofinowski E, Lowe D, Esfandiari MA. Evolution of the earth observing system (EOS) data and information system (EOSDIS). Standard-Based Data and Information Systems for Earth Observation 2010: 63-92.

Ramaswamy V, Muraleedharan PM, Babu CP. Mid-troposphere transport of Middle-East dust over the Arabian Sea and its effect on rainwater composition and sensitive ecosystems over India. Scientific Reports 2017; 7: 13676.

Rashki A, Middleton NJ, Goudie AS. Dust storms in Iran – Distribution, causes, frequencies and impacts. Aeolian Research 2021; 48: 100655.

Revel-Rolland M, De Deckker P, Delmonte B, Hesse PP, Magee JW, Basile-Doelsch I, et al. Eastern Australia: A possible source of dust in East Antarctica interglacial ice. Earth and Planetary Science Letters 2006; 249: 1-13.

Robinson S, Ivanovic R, van de Flierdt T, Blanchet CL, Tachikawa K, Martin EE, et al. Global continental and marine detrital εNd: An updated compilation for use in understanding marine Nd cycling. Chemical Geology 2021; 567: 120119.

Schulz M, Prospero JM, Baker AR, Dentener F, Ickes L, Liss PS, et al. Atmospheric transport and deposition of mineral dust to the ocean: implications for research needs. Environmental Science & Technology 2012; 46: 10390-10404.

Shi J-H, Gao H-W, Zhang J, Tan S-C, Ren J-L, Liu C-G, et al. Examination of causative link between a spring bloom and dry/wet deposition of Asian dust in the Yellow Sea, China. Journal of Geophysical Research: Atmospheres 2012; 117.

Siefert RL, Johansen AM, Hoffmann MR. Chemical characterization of ambient aerosol collected during the southwest monsoon and intermonsoon seasons over the Arabian Sea: Labile-Fe (II) and other trace metals. Journal of Geophysical Research: Atmospheres 1999; 104: 3511-3526.

Singh ND, Singh SK, Malla N, Chinni V. Biogeochemical cycling of dissolved manganese in the Arabian Sea. Geochimica et Cosmochimica Acta 2023; 343: 396-415.

Singh SK, Rai SK, Krishnaswami S. Sr and Nd isotopes in river sediments from the Ganga Basin: sediment provenance and spatial variability in physical erosion. Journal of Geophysical Research: Earth Surface 2008; 113.

Sirocko F. Abrupt change in monsoonal climate: evidence from the geochemical composition of Arabian Sea sediments. Christian-Albrechts-Universität zu Kiel, 1994.

Spooner ETC. The strontium isotopic composition of seawater, and seawater-oceanic crust interaction. Earth and Planetary Science Letters 1976; 31: 167-174.

Stein A, Draxler R, Rolph G, Stunder B, Cohen M, Ngan F. NOAA's HYSPLIT atmospheric transport and dispersion modeling system. Bulletin of the American Meteorological Society 2015; 96: 2059-2077.

Suresh K, Singh U, Kumar A, Karri D, Peketi A, Ramaswamy V. Provenance tracing of long-range transported dust over the Northeastern Arabian Sea during the southwest monsoon. Atmospheric Research 2021; 250: 105377.

Tindale NW, Pease PP. Aerosols over the Arabian Sea: Atmospheric transport pathways and concentrations of dust and sea salt. Deep Sea Research Part II: Topical Studies in Oceanography 1999; 46: 1577-1595.

Tripathi JK, Bock B, Rajamani V. Nd and Sr isotope characteristics of Quaternary Indo-Gangetic plain sediments: Source distinctiveness in different geographic regions and its geological significance. Chemical Geology 2013; 344: 12-22.

Tripathy GR, Singh SK, Bhushan R, Ramaswamy V. Sr–Nd isotope composition of the Bay of Bengal sediments: Impact of climate on erosion in the Himalaya. Geochemical Journal 2011; 45: 175-186.

Turetta C, Zangrando R, Barbaro E, Gabrieli J, Scalabrin E, Zennaro P, et al. Water-soluble trace, rare earth elements and organic compounds in Arctic aerosol. Rendiconti Lincei 2016; 27: 95-103.

Veselovskii I, Goloub P, Podvin T, Tanre D, da Silva A, Colarco P, et al. Characterization of smoke and dust episode over West Africa: comparison of MERRA-2 modeling with multiwavelength Mie–Raman lidar observations. Atmos. Meas. Tech. 2018; 11: 949-969.

Vroon PZ, van Bergen MJ, White WM, Varekamp JC. Sr-Nd-Pb isotope systematics of the Banda Arc, Indonesia: Combined subduction and assimilation of continental material. Journal of Geophysical Research: Solid Earth 1993; 98: 22349-22366.

Wang S-H, Hsu NC, Tsay S-C, Lin N-H, Sayer AM, Huang S-J, et al. Can Asian dust trigger phytoplankton blooms in the oligotrophic northern South China Sea? Geophysical Research Letters 2012; 39.

Whitford DJ. Strontium isotopic studies of the volcanic rocks of the Saunda arc, Indonesia, and their petrogenetic implications. Geochimica et Cosmochimica Acta 1975; 39: 1287-1302.

Yadav S, Rajamani V. Geochemistry of aerosols of northwestern part of India adjoining the Thar desert1 1Associate editor: S. Krishanswami. Geochimica et Cosmochimica Acta 2004; 68: 1975-1988.

Yan Y, Zheng Q, Yu R-l, Hu G-r, Huang H-b, Lin C-q, et al. Characteristics and provenance implications of rare earth elements and Sr–Nd isotopes in PM2.5 aerosols and PM2.5 fugitive dusts from an inland city of southeastern China. Atmospheric Environment 2020; 220: 117069.

Yu Z, Colin C, Wan S, Saraswat R, Song L, Xu Z, et al. Sea level-controlled sediment transport to the eastern Arabian Sea over the past 600 kyr: Clay minerals and SrNd isotopic evidence from IODP site U1457. Quaternary Science Reviews 2019; 205: 22-34.

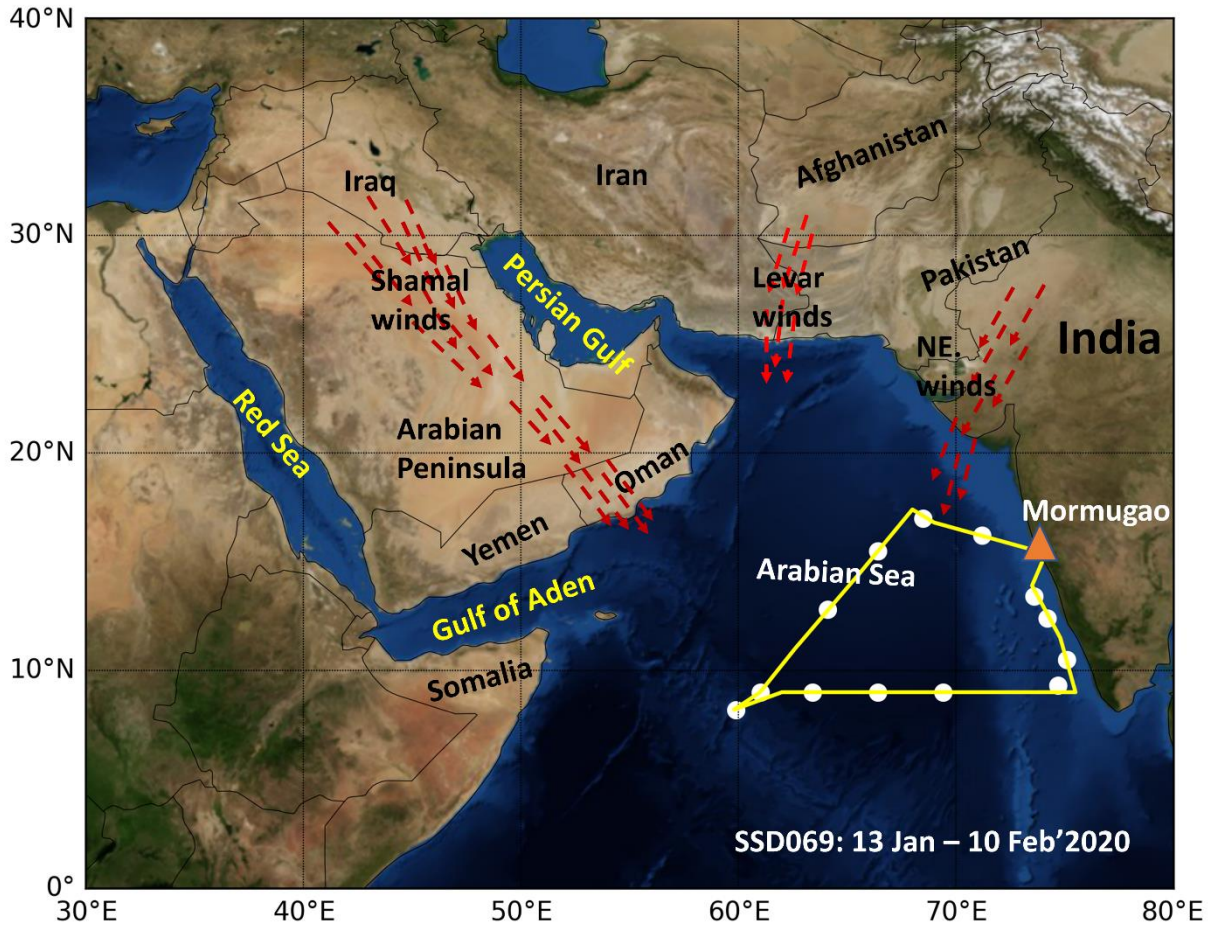

Figure 1. The track used for the dust sample collection in the Arabian Sea during SSD69 cruise (13 January – 10 February 2020).

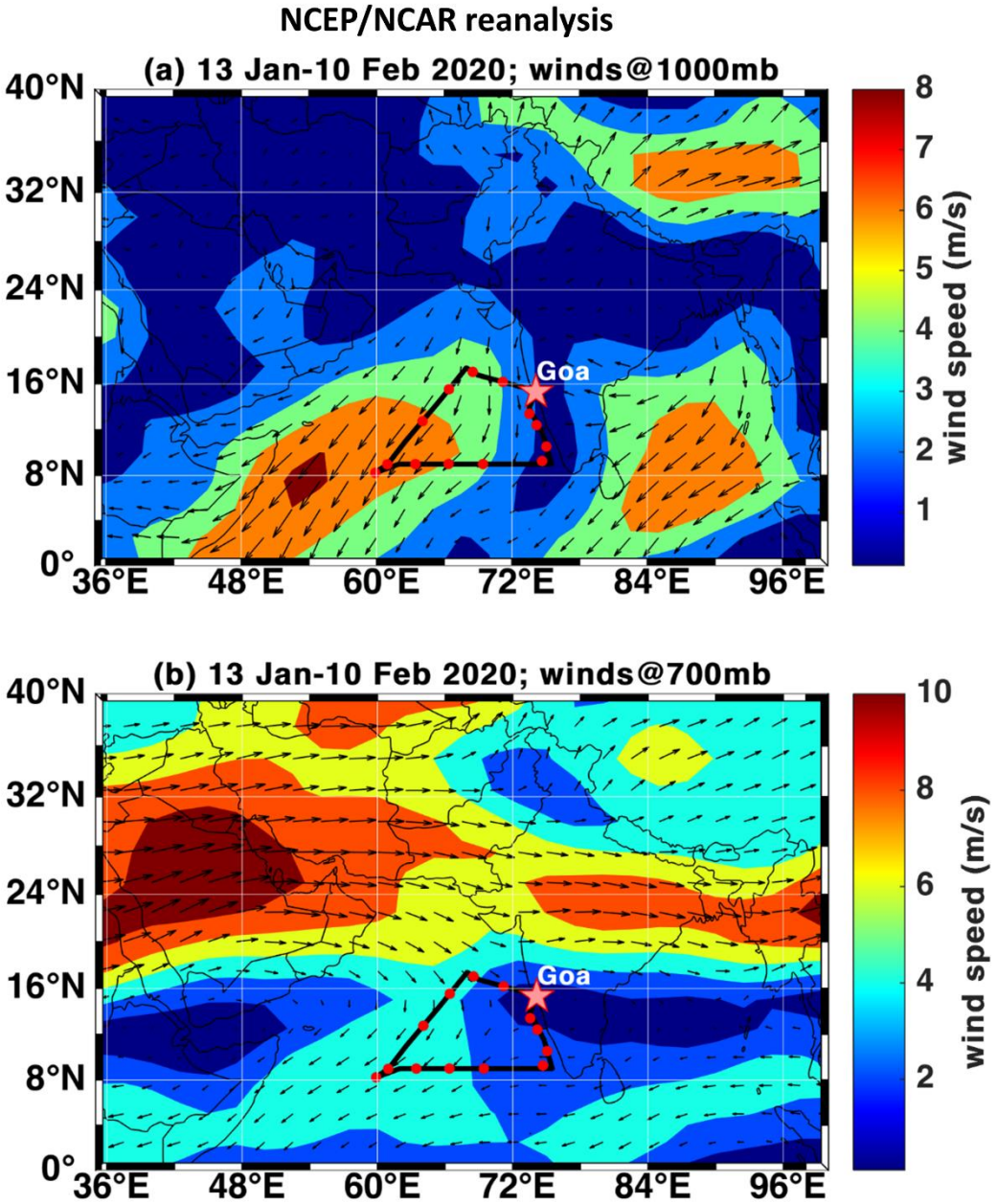

Figure 2. Wind fields over the Arabian Sea at 1000 mb (surface level) and 700 mb (~3 km) during SSD069 cruise (13 January – 10 February 2020).

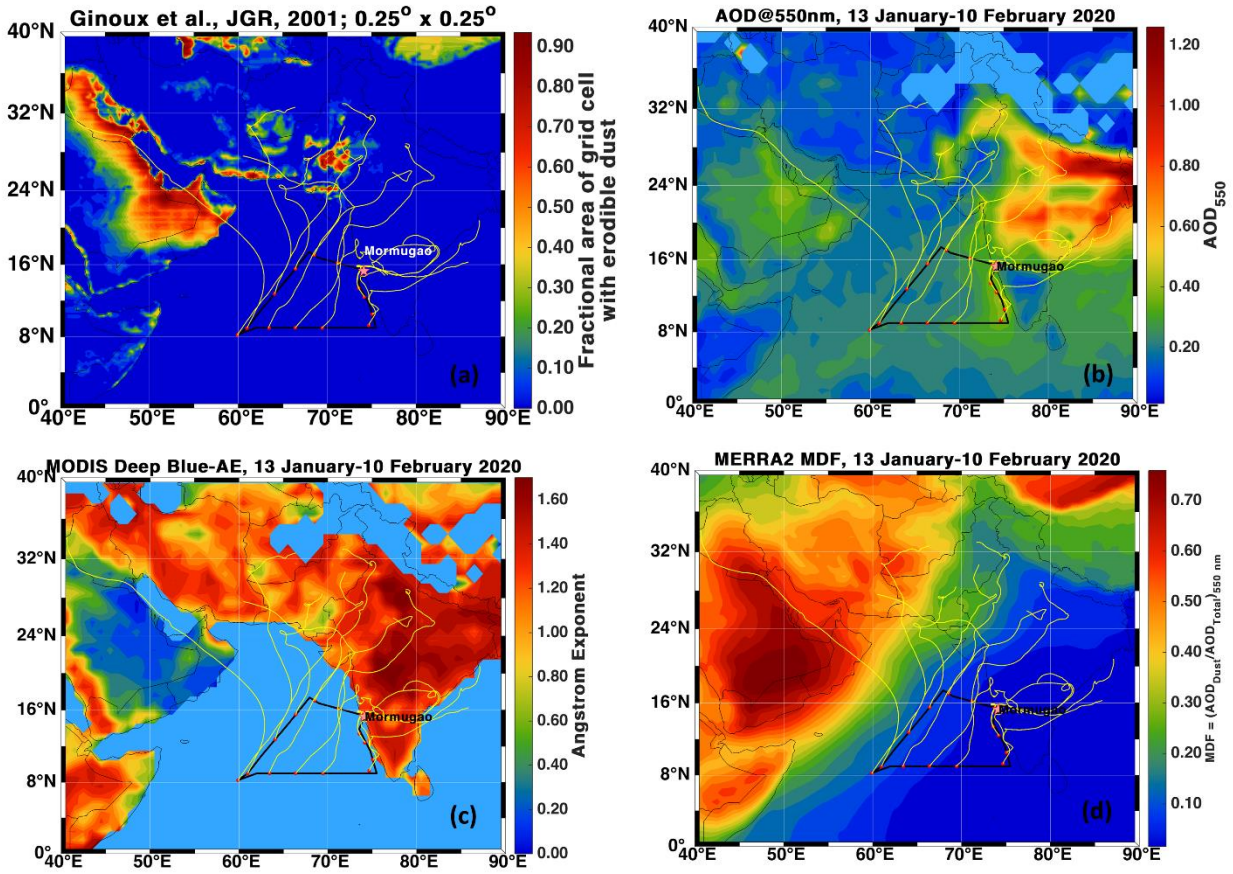

Figure 3. Geographical map containing the Hybrid Single Particle Lagrangian Integrated Trajectory model (HYSPLIT, vers. 4.0) based 7-day isentropic air mass backward trajectories (AMBTs) at an arrival height of 500 m alongside (a) erodible dust fraction, (b) MODIS aerosol optical depth (AOD at 550 nm: combined retrievals of deep blue and dark target algorithms; best suited for dust and other aerosols), (c) MODIS deep blue algorithm based angstrom exponent (AE, 0.412-0.470 µm), and (d) mineral dust fraction (MDF) estimate, the dust to total aerosol optical depth (AOD_{dust}/AOD_{total}) during SSD069 cruise.

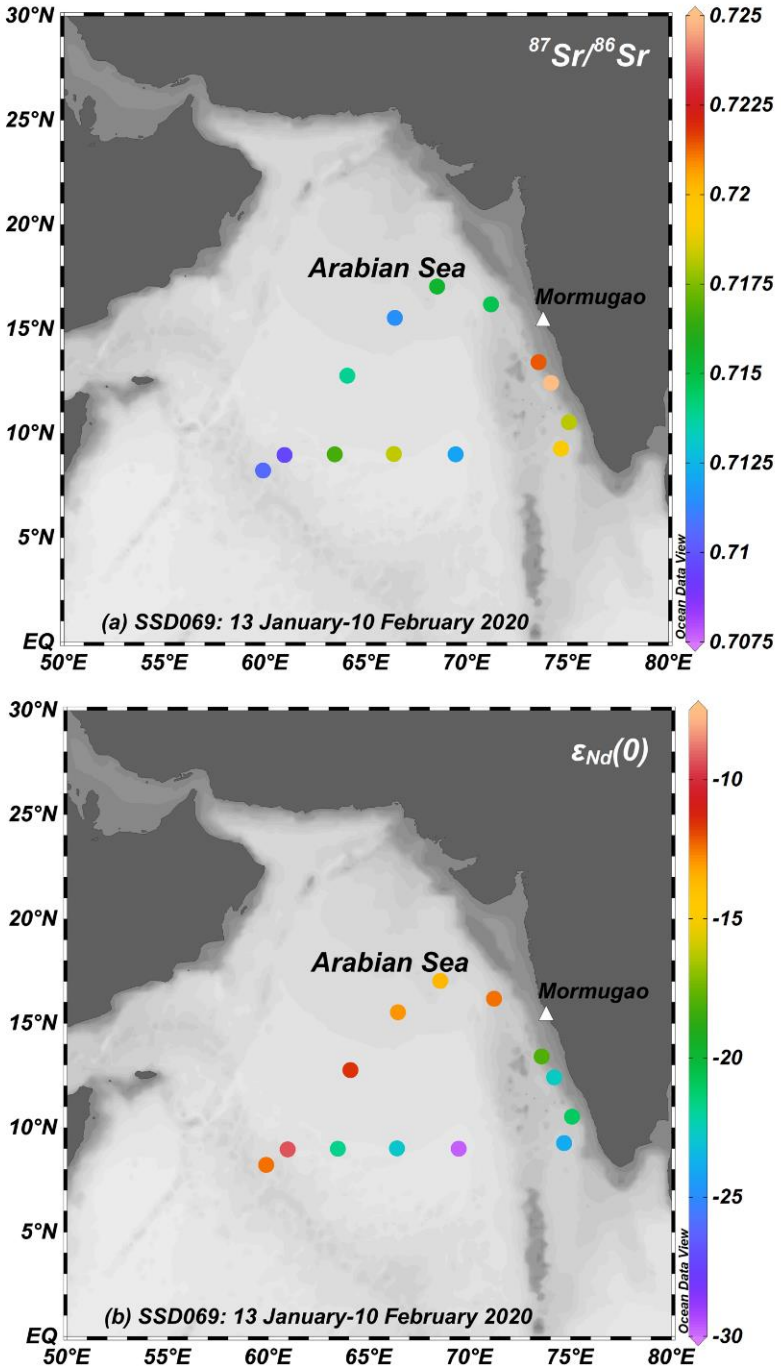

Figure 4. Spatial variability of $^{87}Sr/^{86}Sr$ and (b) $\varepsilon_{Nd}(0)$ of dust samples collected onboard ORV Sindhu Sadhana during SSD069 cruise (13 January – 10 February 2020).

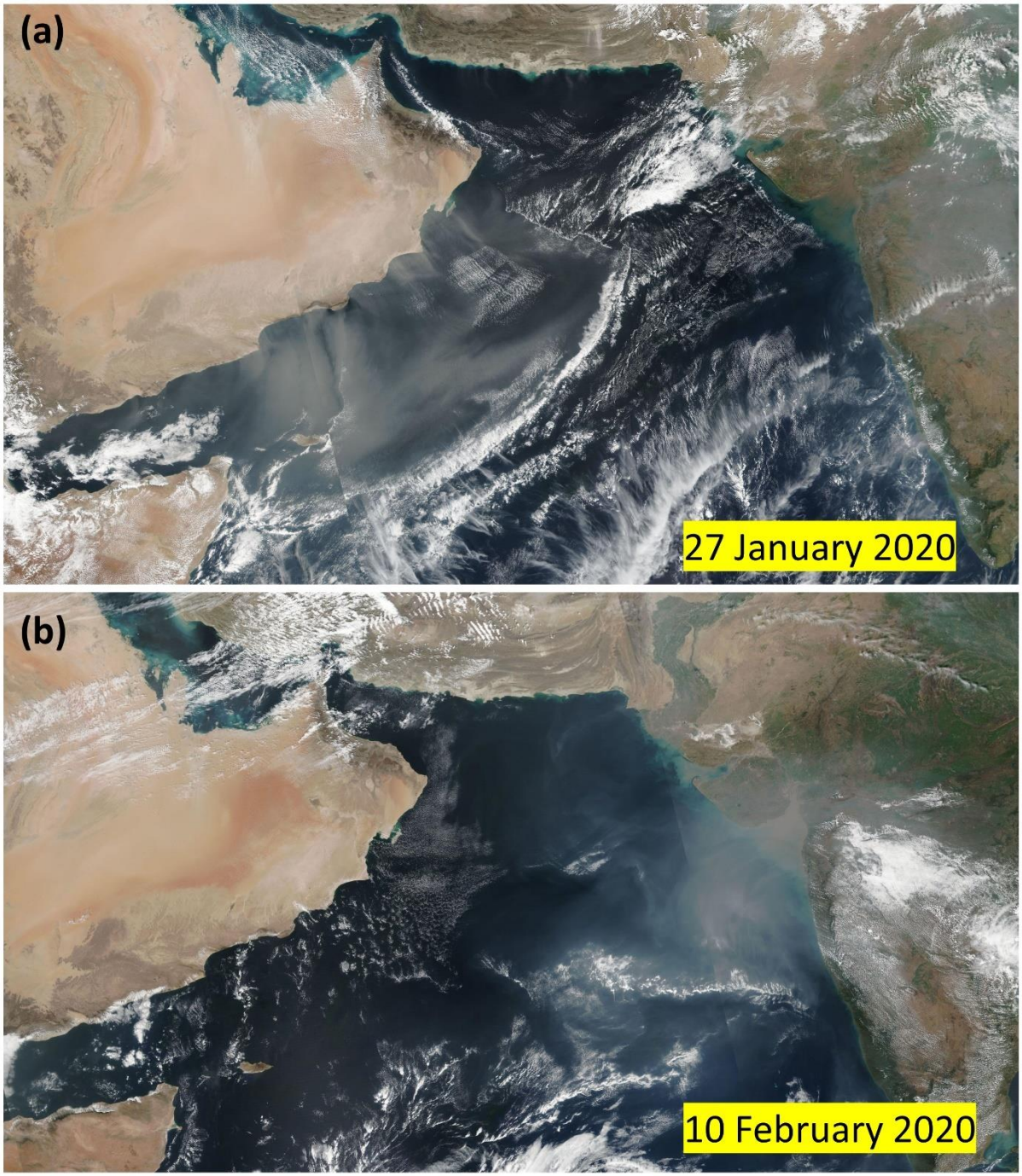

Figure 5. The images of MODIS NPP VIIRS retrieved dust storm events during SSD069 expedition.

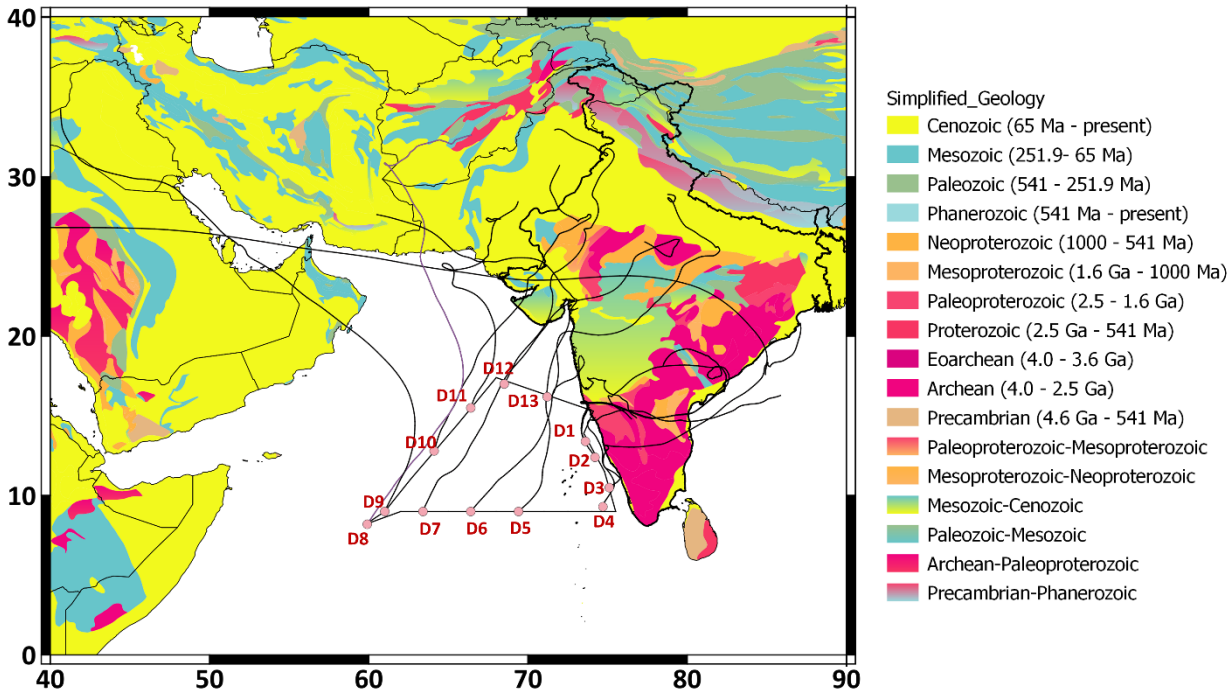

Figure 6. Air mass back trajectories computed using HYSPLIT-4 model at an arrival height of 500 m superimposed upon the simplified geology map according to their ages during SSD069 cruise. The numbers at the midpoint alongside the cruise track correspond to dust samples collected over the Arabian Sea.

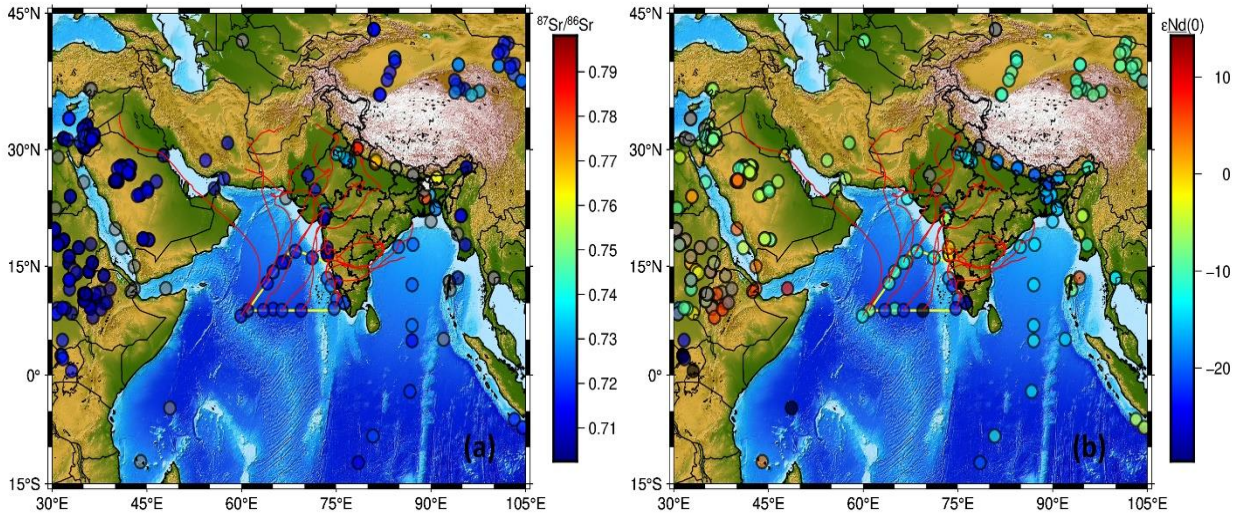

Figure 7. A comparison of $^{87}Sr/^{86}Sr$ (left panel) and $\varepsilon_{Nd}(0)$ (right panel) of the silicate fraction of dust particles collected over the Arabian Sea during SSD069 cruise with those reported for potential dust-source areas (PDA) surrounding this marine basin.

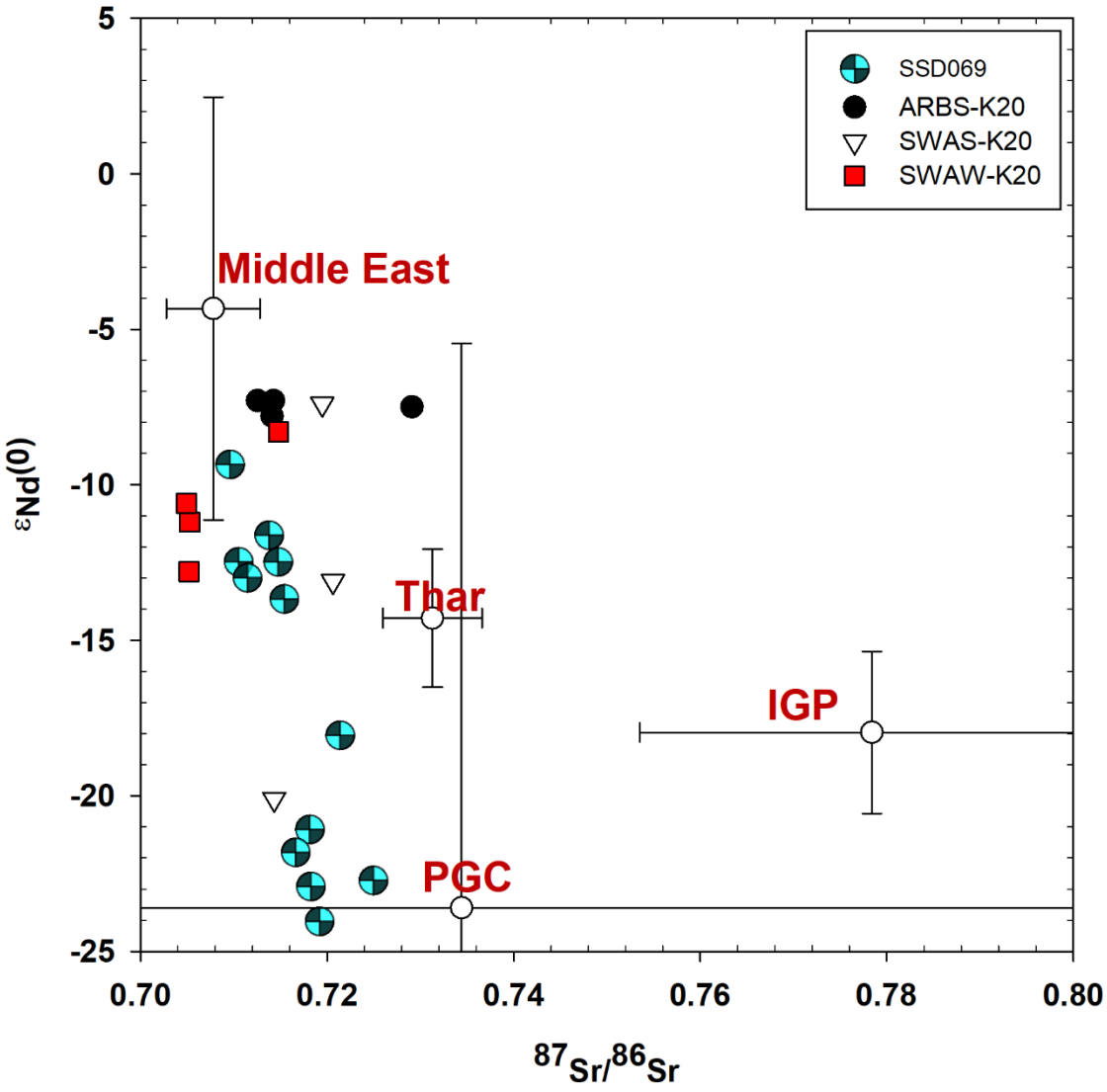

Figure 8. Source apportionment of mineral dust over the Arabian Sea during a winter cruise (SSD069) using the $^{87}Sr/^{86}Sr$ and $\varepsilon_{Nd}(0)$ of the silicate fraction of marine aerosols by comparing with the contributing source profiles (Lightfoot et al., 1990; Tripathi et al., 2013; Kumar et al., 2020; Jewell et al., 2021; Robinson et al., 2021; Kunkelova et al., 2022).

Table 1. Radiogenic isotopic composition of Sr and Nd in the silicate fraction of dust samples collected over the Arabian Sea during SSD069 cruise (10 Jaunary-13 February 2020).

id	Sampling dates	Av. Lat	Av. Lon	Vol.of air (m3)	[Sr] (ng/m^3)	[Nd] (ng/m^3)	$(^{87}Sr/^{86}Sr)_{true}$	$\varepsilon_{Nd}(0)_{true}$	$\delta^{87}Sr$	type
Dust 1	13-13/01/2020	13.40488	73.55026	793.8	7.18	0.53	0.721385	-18.1	17.2	IGP, LH, PGC
Dust 2	13-14/01/2020	12.41089	74.17953	840	9.47	0.75	0.724953	-22.7	22.2	IGP, LH, PGC
Dust 3	14-14/01/2020	10.53557	75.05226	708	13.88	1.11	0.718144	-21.1	12.6	IGP, LH, PGC
Dust 4	14-16/01/2020	9.262292	74.6719	810	9.41	0.72	0.719168	-24.0	14.1	IGP, LH, PGC
Dust 5	18-22/01/2020	8.998432	69.43466	1152	5.99	0.10	0.711996	-29.8#	3.9	n.a.
Dust 6	22-25/01/2020	9.00342	66.3821	996	6.82	0.40	0.718239	-22.9	12.7	IGP, LH, PGC
Dust 7	25-27/01/2020	8.996064	63.44491	1200	7.25	0.32	0.716615	-21.8	10.5	IGP, LH, PGC
Dust 8	27-29/01/2020	8.971341	60.95897	1056	43.40	1.02	0.709573	-9.3	0.5	Arabian Peninsula, Iran
Dust 9	29-31/01/2020	8.225261	59.88377	612	15.54	0.51	0.710501	-12.5	1.8	Arabian Peninsula, Iran
Dust 10	02-04/02/2020	12.75361	64.07361	1590	5.02	0.43	0.713772	-11.6	6.4	Arabian Peninsula, Iran
Dust 11	05-06/02/2020	15.53082	66.41979	978	8.27	0.49	0.711454	-13.0	3.2	Arabian Peninsula, Iran
Dust 12	07-09/02/2020	17.03374	68.52549	420	24.95	1.87	0.715403	-13.7	8.7	Arabian Peninsula, Iran
Dust 13	10-10/02/2020	16.17179	71.19205	696	13.26	1.18	0.714736	-12.5	7.8	Arabian Peninsula, Iran

Note: $\varepsilon_{Nd}(0) = (R_{sample}/R_{CHUR} -1) \times 10000$; R = $^{143}Nd/^{144}Nd$.; Here, CHUR' = Chondritic Uniform Reservoir and has value of 0.512638 ((Jacobsen and Wasserburg, 1980); Probable source is based on the origin of seven day isentropic backward air mass trajectories computed from the HYSPLIT-5 model. Here, # blank correction is more than 50% of the signal detected for this sample and therefore not considered for source apportionment. $\delta^{87}Sr = (R_{sample}/R_{seawater} -1)x1000$; R = 87Sr/86Sr. A A value of 0.7092 has been used for $R_{seawater}$ ((Spooner, 1976)). The acronyms IGP, LH and PGC refer to the Indo-Gangetic Plain, Lesser Himalaya and Peninsular Gneissic Complex, respectively.

Table 2. Representative end member signatures of Sr and Nd isotopic composition from potential dust-source areas surrounding the Arabian Sea.

PDA	**$^{87}Sr/^{86}Sr$**	**$\varepsilon_{Nd}(0)$**	**Reference**
Indo-Gangetic Plain	0.74-0.80	-23- to -18	Singh et al., 2008; Tripathy et al., 2013; Awasthi et al., 2020
Thar Desert	0.7289-0.7390	-15.9 to.-12.6	Yadav et al., 2004
Sistan-Lut Desert (Iran)	0.7098±0.0005	-7.6±0.7	Kunkelova et al., 2022; Kumar et al., 2020
Makran coast (Iran)			Kumar et al., 2020
Arabian Peninsula	0.7115±0.0012	-6.4±1.8	Kunkelova et al., 2022
Mesopotamia (Iraq, Kuwait, Syria)	0.7087±0.0017	-3.5±1.8	Kunkelova et al., 2022; Kumar et al., 2020; Henderson et al., 2020
South Levant	0.7116±0.0011	-6.8±0.7	Kunkelova et al., 2022
Horn of Africa (Somalia)	0.7166, 0.7098-0.7099	-6.59, -8.3 to -6.5	Jung et al., 2004; Sirocko, 1994
Western Sahara	0.7279±0.0052	-14.79±2.16	Jewell et al., 2021
Central Sahara	0.7186±0.0052	-9.96±3.85	Jewell et al., 2021
Eastern Sahara (Egypt, N. Sudan)	0.705-0.724, 0.7059±0.0017 0.7058±0.0014	-12.4 to -10.0, -1.1±2.7 -1.34±2.46	Kunkelova et al., 2022; Scheuvens et al., 2013 Jewell et al., 2021